Electron temperature gradient turbulence

W. Dorland, F. Jenko[*], M. Kotschenreuther[†], B. N. Rogers

Institute for Plasma Research, University of Maryland, College Park, Maryland, 20742, USA

(September 29, 2000)

The first toroidal, gyrokinetic, electromagnetic simulations of small scale plasma turbulence are presented. The turbulence considered is driven by gradients in the electron temperature. It is found that "ETG" turbulence can induce experimentally relevant thermal losses in magnetic confinement fusion devices. For typical tokamak parameters, the transport is essentially electrostatic in character. The simulation results are qualitatively consistent with a model that balances linear and secondary mode growth rates. Significant streamer-dominated transport at long wavelengths occurs because the secondary modes that produce saturation become weak in the ETG limit.

PACS: 52.35.Ra, 52.35.Kt, 52.65.Tt

Understanding and controlling transport which arises from small scale turbulence in magnetized plasma is a central challenge for magnetic confinement fusion research. Here, we present the first toroidal, electromagnetic, gyrokinetic simulations of turbulence driven by electron temperature gradients. Experimentally significant thermal transport is observed when long wavelength toroidal ETG instabilities are unstable. A straightforward model provides insight into why this happens.

The equations which describe electrostatic microinstabilities driven by electron temperature gradients [1–4] (ETG) and by ion temperature gradients (ITG) are very similar. In fact, the linear instabilities are exactly the same, except that the species labels for length and time scales are exchanged. The length scale for each is the Larmor radius of the non-adiabatic species, *i.e.*, ρ_e and ρ_i respectively. The time scales for the two modes are L_{Te}/v_{te} and L_{Ti}/v_{ti}, where L_{Ts} and v_{ts} are the equilibrium temperature gradient scale length and thermal velocity for species s. In a typical fusion plasma, $\rho_i \sim 60\rho_e$ and $v_{te} \sim 60v_{ti}$, so that electron scale turbulence is characterized by shorter wavelengths and higher frequencies. Simple mixing length arguments suggest $\chi_s \sim \rho_s^2 v_{ts}/L_{Ts} \equiv \chi_{s0}$, so that $\chi_i \sim 60\chi_e$.

This disparity in anomalous electron and ion thermal transport is not typically observed in laboratory experiments, suggesting that there could be an important difference between electron- and ion-scale physics. In part, the absence of this disparity arises because significant electron transport is driven by ion-scale turbulence, mostly as a result of the non-adiabatic response of electrons which are trapped in low magnetic field regions. This is the origin of electron thermal transport in the IFS/PPPL [5] model, for example. However, there are experimental cases [6,7] in which distinctly anomalous electron thermal transport is observed without accompanying anomalous ion thermal transport or ion-scale fluctuations. Here, we address the basic questions of whether ETG turbulence is a reasonable candidate for explaining experimental observations such as these, and if so, why.

ETG instabilities are characterized by $k_\theta \rho_e \sim 1$, where k_θ is a typical poloidal wavenumber of an eddy. Because $k_\perp \rho_i \gg 1$, the ion response to a perturbation is adiabatic: $n_i \sim \exp\{-Z|e|\Phi/T_i\}$. As a consequence, ETG turbulence drives no particle transport. Instead, it produces primarily electron thermal flux and possibly current diffusion. Here, $k_\perp$ is a typical wavenumber of the perturbation in the plane perpendicular to the magnetic field, $Z|e|$ is the ion charge, Φ is the fluctuating electrostatic potential, and T_i is the ion temperature.

The literature suggests that ETG transport could be (a) of modest size, by analogy [8] with electrostatic ITG simulations ($\chi_e \sim \chi_{e0}$), (b) near experimental levels because of electromagnetic effects, with $\chi_e \sim \chi_{e0}/\beta$ [2–4], where β is the ratio of plasma and magnetic pressures, or (c) potentially very large, because of the formation of radially extended eddies ("streamers") [9,10] whose growth is limited by secondary instabilities. Our simulations support the latter view. We also identify the dominant secondary instabilities which lead to nonlinear saturation, and the tertiary instabilities that limit the amplitude of zonal flows.

Electromagnetic, weakly collisional ETG turbulence satisfies the nonlinear gyrokinetic [11,12] ordering. We use two independently developed parallel codes [13] to simulate the gyrokinetic Vlasov-Maxwell system, GENE and GS2. Each evolves a five dimensional perturbed distribution function $f = f(\mathbf{x}, \epsilon, \mu)$ on a fixed grid. GENE is the gyrokinetic generalization of a drift kinetic code [14]. GS2 is the nonlinear generalization of a standard gyrokinetic microstability code [15]. In each code, field-line following coordinates (x, y, z) are used to describe turbulence in a tube of magnetic flux [16,10,17]. Periodic boundary conditions which take into account the twist of the magnetic field are used to prevent quasilinear flattening of the driving gradients [16]. The simulation results presented here do not include $\delta B_\parallel$ since $\beta \ll 1$; GENE simulations also ignore trapped particles. We employ a high aspect ratio MHD equilibrium characterized by magnetic shear $\hat{s}$, normalized beta gradient α, and minor/major radius r/R. Reference parameters are safety factor $q = 1.4$, $\hat{s} = 0.8$, $R/L_T = 6.9$, $R/L_n = 2.2$, $T_i = T_e$, $Z_{\text{eff}} = 1$, $\alpha = 0.45$, and $r/R = 0.18$. Here, L is an equilibrium temperature or density scale length. A typical simula-

tion domain has $L_x = 175\rho_e$, with $1 < L_x/L_y < 4$, and $\Delta_x = \Delta_y = 1.8\rho_e$. Along the field line, there are 16-32 gridpoints per 2π. The velocity space grid is typically 50×10. Strongly turbulent ETG runs require $\sim 10^5$ dynamically adjusted time steps.

The turbulent electric and magnetic fields induce radial thermal transport Q (defined in Ref. [13]). The thermal diffusivity is defined by $\chi = Q/(-n^{(0)}\nabla T^{(0)})$, in units of χ_{s0}. As a check on the numerics, we have successfully benchmarked GS2 and GENE for parameters similar to the reference parameters. Also, GS2 reproduces [lower curve, Fig. (1), $\chi_i = 0.8\chi_{i0}$] the transport measured in gyrokinetic particle-in-cell simulations [18] of electrostatic ITG turbulence.

The turbulent thermal diffusivities *vs.* time shown in Fig. (1) are typical. The upper curve (normalized to χ_{e0}) is from an electromagnetic ETG simulation. The lower curve (normalized to χ_{i0}) is from an electrostatic ($\alpha = 0$) ITG simulation. The larger normalized electron thermal flux indicates that turbulence on ion and electron scales is essentially different, and that ETG turbulence may be strong enough to induce thermal losses of the same order as ITG turbulence. We observe that large normalized ETG thermal transport is associated with high amplitude, radially elongated streamers at the outboard midplane in the turbulent steady state [Fig. (2)].

The simulations do not support the model of Ref. [19], which predicts large ETG transport from the magnetic nonlinearity. In 16 finite β simulations [Fig. (3)], each with $\beta \leq 10\%$, we observe that the ETG heat flux is predominantly electrostatic, even when the peak in the fluctuation spectrum lies close to $k_\perp\delta$, where δ is the collisionless skip depth. The contribution from magnetic flutter is at most a few percent of the total heat flux.

We now turn to a model related to ideas in Refs. [10,20] which provides insight into the simulation results. Given a finite amplitude linear eigenmode (the "primary" instability), we identify "secondary" instabilities, whose growth rates increase with the amplitude of the primary. The secondary instabilities eventually grow faster than the primary mode, until they reach nonlinear amplitudes and saturate the primary mode. Sheared zonal flows are created from the breakup of the primary modes. These flows contain a linearly undamped component that could persist in the turbulent state, lowering the saturation level [21,18,22]. We also identify "tertiary" instabilities, which limit the amplitude of the zonal flows. Tertiary growth rates are proportional to the amplitude of the zonal flows. In contrast to the ITG system [22], the dynamics of secondary and tertiary modes in the ETG system are similar.

First addressing the dynamics of secondary modes, we consider a simple limit of electron gyrofluid equations [23]. In the limit of a large amplitude primary, the sound wave coupling and background gradients may be neglected. The guiding center electron density, perpendicular temperature, and electrostatic potential satisfy

$$\frac{dn}{dt} + \frac{1}{2}\left[\nabla_\perp^2\psi, T_\perp\right] = 0 , \quad n = \left[\tau - (1 + \tau)\nabla_\perp^2\right]\psi, \quad (1)$$

and $dT_\perp/dt = 0$, where $d/dt = \partial/\partial t + [\psi, \cdot]$, and terms of order $(k_\perp\rho)^4$ have been neglected. (Earlier treatments [9,10] along the lines of the present model neglected the polarization drift; without it, the present secondary instability is missing, so that simulations may fail to saturate.) As in Ref. [22], the relative phase of the temperature and density perturbations in the ETG eigenmode is such that the perpendicular temperature dynamics do not significantly affect the results, so we neglect $T_\perp$ here. Length scales are normalized to ρ_e, $\tau = Z_{\text{eff}}T_{e0}/T_{i0}$, $n = n_{phys}L_{Te}/(\rho_e n_0)$, and $\psi = e\psi_{phys}L_{Te}/(\rho_e T_{e0})$.

Ignoring magnetic shear, we consider the linearization $\psi = \psi_p(y) + \tilde{\psi}(y)\exp(\gamma t + ik_x x)$, in which a crude model of the primary mode structure is given by $\psi_p(y) = \psi_{p0}\cos(k_p y)$. Here, k_p represents the primary's poloidal wavenumber and ψ_{p0} determines its amplitude. One finds

$$\left[\left(\frac{\tau}{1 + \tau}\right)\gamma + k_x^2\bar{\gamma}\right]\tilde{\psi} = \partial_y\left[\bar{\gamma}^2\partial_y(\tilde{\psi}/\bar{\gamma})\right] \quad (2)$$

with $\bar{\gamma} = \gamma - ik_x\psi_p'(y)$. The ETG secondary equation differs from conventional Kelvin-Helmholtz (KH) because of the first term on the left-hand side (the ion response). Balancing this term with the other terms in Eq. (2) leads to a maximum growth rate $\sim k_p^4\psi_{p0}$ for $k_x \sim k_p$. This growth rate is a factor of $(k_\perp\rho_e)^2$ smaller than conventional KH. Relative to ITG modes, whose secondary instability growth rates exceed conventional KH [22], secondary instabilities of ETG modes are quite weak, particularly for small $k_\perp\rho_e$. This weakening of the secondary instabilities is the main reason that ETG turbulence saturates at high normalized levels for some parameters.

A closed form solution of Eq. (2) exists in the limit $(k_x \ll k_p \ll 1)$, with eigenvalue $\gamma = \Gamma k_p^4(1 + \tau^{-1})\psi_{p0}$, $\Gamma = (k_x/k_p)^2/\sqrt{2}$. For the less restrictive limit $k_p \ll 1$, Γ may be found numerically [Fig. (4)]. Also shown is the radial component of the velocity of the eigenmode for $k_x/k_p = 0.75$, with $k_p = 0.1$. Boundary layers form at the nulls $\psi_p'(y) = -k_p\psi_{p0}\sin(k_p y)$, where the coefficient of the highest derivative term, $\bar{\gamma} = \gamma - ik_x\psi_p'(y)$, becomes very small ($\bar{\gamma} = \gamma$). The width of these layers is given by $k_p\Delta y \sim \gamma/(k_x k_p\psi_{p0}) \sim 0.2(1 + \tau^{-1})k_p^2 \ll 1$. To accurately resolve these quasi-singular regions for a given $k_p\rho_e$ requires $k_y\rho_e^{\text{max}} \sim (k_p\rho_e)^{-1}$, a challenging requirement in a simulation with unstable toroidal ETG modes in the range of $k_p\rho_e \sim 0.1$. Fortunately, one can show the growth rate is insensitive to the detailed eigenmode stucture in these singular regions. Moreover, higher order FLR effects, neglected in this simple model, further reduce the sensitivity.

For $\hat{s} \neq 0$, the primary modes twist with the field lines, causing the physical $k_\perp^2$ to exceed $k_x^2 + k_y^2$. This effect, which tends to enhance the growth rate of secondary modes, is reduced by the decrease in the primary mode amplitude along the field lines, and by higher order FLR

terms not included here. We find the net result is typically a modest enhancement in γ and unstable k_x. To understand this, the previous analysis can be generalized to allow for $\partial_z \neq 0$. Again considering large primary mode amplitudes, one finds the leading order growth rates of the 2D secondary modes are given by the generalization of Eq. (2) with $\partial_x^2 + \partial_y^2 \rightarrow \nabla_\perp^2 = (\partial_x + \hat{s}\theta\partial_y)^2 + \partial_y^2$:

$$\left[\left(\frac{\tau}{1+\tau} \right) \gamma + (1 + \hat{s}^2\theta^2)\bar{\gamma}'' \right] \tilde{\psi} = \bar{\gamma}\nabla_\perp^2 \tilde{\psi}, \qquad (3)$$

where $\theta = 2\pi q R z$. The eigenmodes modes are localized in θ (or z) at θ-values satisfying $\partial_\theta\gamma = 0$. Applying the transformation $\hat{\psi} = e^{-icy}\tilde{\psi}$, $c = -k_x\hat{s}\theta/(1 + \hat{s}^2\theta^2)$ to Eq. (3) and defining $\hat{k}_x^2 = k_x^2/(1 + \hat{s}^2\theta^2)$ and $\hat{k}_p^2 = k_p^2(1 + \hat{s}^2\theta^2)$, Eq. (2) is recovered with hatted variables. Consistent with this, solving Eq. (3) numerically with periodic boundary conditions, we obtain maxima in the growth rate at discrete values of θ and $\hat{k}_x \sim \hat{k}_p$, with $\gamma_{max} \sim \hat{k}_p^4\psi_{p0}$ (the same as before). Maximizing this over a toroidal ETG mode eigenfunction typically yields less than a factor of two enhancement in γ and the associated unstable k_x.

The predictions of the models just described are in reasonable agreement with the secondary instability growth rates observed in nonlinear gyrokinetic ETG simulations. For example, for the reference parameters (except $\alpha = \beta = 0$) with $k_p\rho_e = 0.2$ and $k_x\rho_e = 0.5$, we find $\Gamma \sim 0.3$, compared with the expected $\Gamma \sim 0.2$.

Balancing the primary and secondary mode growth rates produces a scaling for the normalized saturation level of the primary modes, $\phi_{\text{sat}} \sim \gamma_l/k_\perp^4$. For comparison with nonlinear simulation results described in more detail elsewhere [13], we maximize this expression over k_x and k_y using the growth rate of the toroidal ETG mode, and evaluating $k_\perp^4$ by squaring the average $k_\perp^2$ defined in Ref. [5]. Representative curves are shown in Fig. (5). The simple model predicts the region of high transport seen in Fig. (3) reasonably well. Physically, high transport is predicted when the dominant modes shift to longer wavelengths. For $\gamma \sim \sqrt{\omega_d\omega_*\eta_e} - k_\parallel v_t$, instability requires $k_p\rho_e \gtrsim L_T/(qR)$. Small L_n/R can be strongly stabilizing [24].

Without curvature, we find that electromagnetic ETG turbulence saturates at low levels, $\chi_e \sim \chi_{e0}$. We note that unlike toroidal modes, slab eigenmodes necessarily have finite $k_z \neq 0$. As a result, the saturation of slab modes may be controlled by a different secondary instability [10]. Because our slab simulations are qualitatively different and saturate at low levels, we did not include slab ETG instabilities in the maximization of $\gamma/k_\perp^4$ described above.

The nonlinear development of the secondary instabilities leads to the production of zonal flows, which are subject to tertiary instabilities. Ignoring the effects of background gradients, rotational symmetry of Eq. (1) in the perpendicular plane means that Eq. (2) also describes tertiary instabilities in ETG turbulence, so that secondary and tertiary modes in ETG turbulence are both weak. By contrast, the nature of the adiabatic electron response in ITG turbulence breaks this symmetry, so that while tertiary instabilities in the ITG system are weak, the secondary instabilities are strong. [22] This is consistent with the larger normalized transport observed in ETG simulations. To date, we have not observed zonal flow accumulation in simulations with adiabatic ions.

To summarize, we have addressed questions raised by experimental evidence of anomalous electron transport in the absence of ion-scale turbulence. We presented gyrokinetic simulations of ETG turbulence. Our simulations are fully toroidal and electromagnetic. We have shown that ETG turbulence, which cannot be easily stabilized by equilibrium scale $\mathbf{E} \times \mathbf{B}$ shear because of much higher growth rates, and despite its characteristic small scales, is a plausible candidate for explaining these experimental observations. The high normalized saturation amplitude is associated with the observation of radially extended streamers. By identifying the important secondary and tertiary instabilities, we explained key features of these structures, and thus explained why normalized ETG transport can be much larger than normalized ITG transport, despite the fact that the linear instabilities are mathematically identical. Significant streamer-dominated transport at long wavelengths occurs because the secondary modes that produce saturation become weak in the ETG limit.

Important questions remain unanswered. We have not undertaken quantitative comparisons with experimental data. Our model implies the need for careful box-size scalings and multiple species simulations to pin down the actual predicted value of χ_e^{ETG}. Finally, interactions between ETG turbulence and longer wavelength instabilities require investigation.

[1] B. Coppi and G. Rewoldt, in *Advances in Plasma Physics*, edited by A. Simon and W. B. Thompson, volume 6, page 421, John Wiley and Sons, New York, 1976.

[2] Y. C. Lee, J. Q. Dong, P. N. Guzdar, and C. S. Liu, Phys. Fluids **30**, 1331 (1987).

[3] P. N. Guzdar, C. S. Liu, J. Q. Dong, and Y. C. Lee, PRL **57**, 2818 (1986).

[4] W. Horton, B. G. Hong, and W. M. Tang, Phys. Fl. **31**, 2971 (1988).

[5] M. Kotschenreuther, W. Dorland, G. W. Hammett, and

M. A. Beer, Phys. Plasmas **2**, 2381 (1995).

[6] M. Zarnstorff, Bull. Am. Phys. Soc. **43**, 1635 (1999).

[7] B. W. Stallard, Phys. Plasmas **6**, 1978 (1999).

[8] R. E. Waltz, G. M. Staebler, W. Dorland, M. Kotschenreuther, and J. A. Konings, Phys. Plasmas **4**, 2482 (1997).

[9] J. F. Drake, P. N. Guzdar, and A. B. Hassam, PRL **61**, 2205 (1988).

[10] S. C. Cowley, R. M. Kulsrud, and R. Sudan, Phys. Fluids B **3**, 2767 (1991).

[11] T. Antonsen and B. Lane, Phys. Fluids **23**, 1205 (1980).

[12] E. A. Frieman and L. Chen, Phys. Fluids **25**, 502 (1982).

[13] F. Jenko, W. Dorland, M. Kotschenreuther, and B. N. Rogers, Phys. Plasmas **7**, 1904 (2000).

[14] F. Jenko, Comput. Phys. Commun. **125**, 196 (2000).

[15] M. Kotschenreuther, G. Rewoldt, and W. M. Tang, Comp. Phys. Comm. **88**, 128 (1995).

[16] M. A. Beer, S. C. Cowley, and G. W. Hammett, Phys. Plasmas **2**, 2687 (1995).

[17] K. V. Roberts and J. B. Taylor, Phys. Fluids **8**, 315 (1965).

[18] A. M. Dimits et al., Phys. Plasmas **7**, 969 (2000).

[19] W. Horton et al., Phys. Fluids B **4**, 953 (1992).

[20] B. N. Rogers and J. F. Drake, PRL **79**, 229 (1997).

[21] M. N. Rosenbluth and F. Hinton, PRL **80**, 724 (1998).

[22] B. N. Rogers, W. Dorland, and M. Kotschenreuther, PRL (2000).

[23] W. Dorland and G. W. Hammett, Phys. Fluids B **5**, 812 (1993).

[24] F. Romanelli and S. Briguglio, Phys. Fl. B , 754 (1990).

FIG. 2. Characteristic ϕ contours in the outboard x-y plane. This snapshot was taken at the end of the ETG run shown in Fig. 1. The figure is $256\rho_e \times 64\rho_e$.
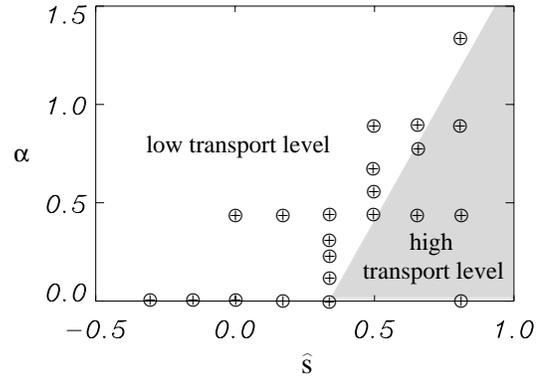
FIG. 3. (a) Nonlinear simulation results for the reference parameters as a function of $\hat{s}$ and α.
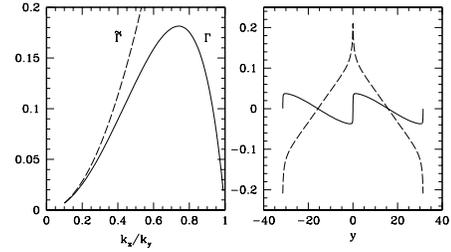
FIG. 4. Secondary instability of long wavelength ETG modes. (a) Growth rate (b) eigenmode (for $k_x/k_p = 0.75$).

FIG. 1. χ_e^{ETG} (upper curve) and χ_i^{ITG} (lower curve) for similar parameters.
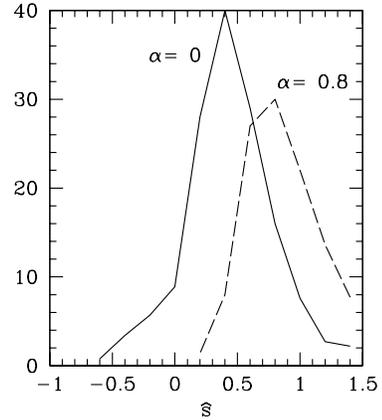
FIG. 5. $\gamma/k_\perp^4$, evaluated for the reference parameters, with varying $\hat{s}$ and α.

4